Implementation of a flexible real-time radar architecture of vital signs based on cyclic temporal moment algorithms using SDR technology

Fatima Sekak, Fouzia Elbahhar, Madjid Haddad

Received XX Month, XXXX; revised XX Month, XXXX; accepted XX Month, XXXX; Date of publication XX Month, XXXX; date of current version XX Month, XXXX.

Digital Object Identifier 10.1109/OJIM.2022.1234567

Implementation of a flexible real-time radar architecture of vital signs based on cyclic temporal moment algorithms using SDR technology

Fatima SEKAK*, Fouzia ELBAHHAR *, and Madjid HADDAD †

[1]Groupe LEOST (Electronic Wave and Signal Laboratory for Transport), University of Gustave Eiffel, F-59666 Villeneuve d' Ascq, France
[2]Segula Engineering France, 92500 Rueil-Malmaison, France

Corresponding author: Fatima Sekak (e-mail: fatima.sekak@gmail.com)

This work has received support from Segula Technologies (www.segulatechnologies.com).

ABSTRACT This paper presents a low-cost bistatic radar built using Software-Defined Radar (SDR) for real-time monitoring and detection of mechanical vibrations and physiological movements of a person's chest. The proposed prototype is based on the complex received signal, which contains information about the heartbeat and respiration rates. Various algorithms can be employed for this purpose, and the choice depends on factors such as accuracy, computational efficiency, and the application's specific requirements. This study aims to evaluate and validate our signal processing solutions based on second-order cyclostationarity algorithms to distinguish cycle frequencies, using a low-cost Universal Software Radio Peripheral (USRP) SDR board. This device provides a software-defined RF architecture to prototype a vital signs radar with custom signal processing. The design concept for breathing and heart rates was implemented and evaluated on a 5.8 GHz SDR platform (USRP2901) using GNU Radio combined with Python blocks. To verify the detecting performances of the proposed prototype, a series of simulations and experiments were conducted on different persons under tests to validate the theory. Moreover, two types of antennas were used: an industrial horn antenna and a patch antenna developed in our laboratory. The results were compared to a reference system, a pulse oximeter, to validate the performances of the algorithm. The respiration and heartbeat rates were correctly estimated for all the subjects with both antennas.

INDEX TERMS SDR; USRP; Microwave radar; vital signs; respiration rate; heart rate; cyclostationary; second-order cyclic moment.

I. INTRODUCTION

SURVEILLANCE of health is a key aspect of elderly care and imperative for proactive measures, particularly when the early identification of potential risks or diseases can mitigate long-term suffering and medical expenses. Non-contact monitoring of vital signs is crucial for elderly individuals who cannot accept contact measurement due to comfort and compliance issues. Sensitive or fragile skin makes contact-based devices uncomfortable or even painful, leading to poor compliance with health monitoring routines. Additionally, continuous use of contact sensors can cause skin irritation or infections, particularly in elderly individuals with delicate skin or compromised immune systems. Non-contact methods eliminate these risks, providing a safer and easier alternative, especially for those with mobility issues or cognitive impairments. Furthermore, non-contact monitoring reduces anxiety associated with frequent physical examinations or the presence of medical devices, promoting a less intrusive experience. Enhanced hygiene is another benefit, as non-contact systems reduce the risk of cross-contamination, particularly in communal living environments. By minimizing the need for caregiver assistance, these systems also help elderly individuals maintain independence and autonomy.

Monitoring vital signs such as heart and breath rates yields crucial insights into an individual's overall physical

This work is licensed under a Creative Commons Attribution 4.0 License. For more information, see https://creativecommons.org/licenses/by/4.0/

well-being. The use of radar technology for non-invasive and non-contact detection of respiration and heart rates has garnered substantial attention, driven by the increasing demand for non-contact and continuous health monitoring devices. The continued extraction of this important component has pushed development in various possible ways. Considering RF techniques, the body's surface, and the geometric mean of the reflected signal, conventional RF-based vital signs monitoring are also an area of research fueled by the demand for non-contact and continuous health monitoring devices. Various technologies and signal processing techniques are being investigated for this purpose, such as Radar-based techniques, which have contributed to research projects since 1975 [1]. Different radar setups operating at various frequency bands have been historically reported to detect human vital signs, analyzing the interaction between radio-frequency signals and physiological movements, without requiring contact with the human body. In [2] [3] [4], different types of continuous wave (CW) and frequency-modulated continuous wave (FMCW) radars are presented. In [5], the movement of the subject's chest induced by the heartbeat is recorded via an FMCW radar correlated with the electrical signal of the heart, recorded via an ECG acquisition board. This study is conducted on apnea recordings to remove the impact of breathing on the movement of the chest. Quadrature CW radar with I/Q channel demodulation has been proposed in [6]. In [7] [4], a vector network analyzer (VNA) system was reported, which tunes both frequency and power to determine the optimum frequency and minimum power required to extract vital signs. Besides the vector network analysis alternative microwave interferometric radar technique of the VNA was also presented in [8], [9], where the architecture of the six-port receiver is used as an interferometer, for angle, displacement, and vibration measurements. Ultra-Wide Bandwidth (UWB) pulses were employed to detect the heart and breath rates by transmitting very short and repetitive waveforms toward the target person's chest surface [10], [11]. In [12], [13], continuous monitoring of vital signs using an Impulse-Radio (IR) UWB radar has been explored. The echoes are received by a round-trip time delay proportional to the chest surface movement which is based on the phase-shift information introduced by the modulated time delay. Currently, these systems are not available on the market.

Previous studies have demonstrated that non-contact vital signs detection can be achieved using RF signals. However, it can be challenging to distinguish small mechanical vibrations, such as heartbeat and breathing, from low-frequency RF signals. Additionally, most validation tests involve bulky equipment, making it difficult to implement and test in real-time scenarios. Another technologically advanced solution is provided by software-defined radar platforms (SDR). These concepts have gained significant interest in the wireless communication and radar communities due to low-cost implementation, where all operations and functions are fully implemented and easily modified through software. It also allows for the evaluation and comparison of various radar techniques using the same hardware components. For the evaluation, multiple radar system prototypes using SDR have been studied. The SDR radar concept was first introduced by the author of [14]. This new radar parading provides a solution for designing compact radar systems that can easily modify their capabilities without changing the hardware configuration. As a result, the monitoring accuracy is dependent on the SDR transmit/receive setting, and the capabilities of the SDR radar approach have been demonstrated in the literature [15]–[17]. Its application to vibration detection has been first demonstrated by the authors of [18]–[20], and has also been recently explored by the authors of [21]–[23]

In [24], an implementation of a simple respiratory and heart rate monitor application using the Ettus X310 card and GNU Radio and a commercial-off-the-shelf (COTS) SDR. In [25] a sub-6 GHz breathing sensor a universal software radio peripheral (USRP) B205-mini device is presented. This system estimates the channel phase shift and detects low-frequency oscillations in the estimated phase shift. Finally, [26] proposes a system operating at 2.4 GHz based on the USRP 2901 programmed with LabView.

In RF systems, the phenomenon of multipath propagation plays a crucial role in signal transmission. When a signal travels from a transmitter to a receiver, it encounters various obstacles. It reflects off surfaces, leading to multiple signal versions arriving at the receiver through different paths. This multipath effect introduces variations in signal strength, phase, and arrival time, which can significantly impact the received signal's characteristics.

In this paper, unlike many reported SDR systems, our proposed system is not based on distance measurements or channel phase shift estimation and it doesn't require any type of frequency sweep instead. It is based on the complex received signal that contains all the information sought needed to evaluate and validate our signal processing solutions using cyclostationarity algorithms on a low cost SDR board. We implement and evaluate our design concept for breathing and heart rate detection and estimation on the 5.8 GHz software-defined radio platform USRP2901 and GNU Radio combined with python blocks. GNU Radio combined with Python provides the infrastructure to quickly implement the signal processing algorithm based on second-order cyclostationary [27], [28], simplifying the development process and accelerating the experimental validation of new techniques.

The remainder of this paper is organized as follows. Section II explains the model simulation and provides a very brief background behind the second-order cyclostationary algorithm that will be implemented in the radar hardware.

The section IV investigates the simulation result on the GNU Radio platform with Python blocks. Then in the last section, the measurement tests and experimental validation results on human subjects are reported and discussed.

II. THEORETICAL BACKGROUND

Respiration rate (RR) and heart rate (HR) are considered the most important physiological parameters indicating the body's functioning state. The movement of the left ventricle of the heart within the chest is the primary cause of chest movement due to heartbeats. The contraction of the diaphragm during inhalation causes the air to flow into the lungs and pushes the abdomen and ribs outward resulting in chest expansion due to respiration. The chest movements caused by heart beating and breathing are $x_{HR}(t) = x_r + x_h$. It denotes the displacement generated by respiration and heartbeat x_r and x_h, respectively [4].

The proposed concept for the detection of RR and HR has been implemented using the GNU-Radio software and the USRP 2901 as a suitable SDR platform. The SDR provides flexibility and reconfigurability to update processing parameters depending on the environment or the conditions. GNU Radio is an open-source software-defined radio project and the USRP is hardware designed specifically for use with the GNU Radio software. This combination has been used to implement a low-cost radar, which will be presented in this paper. The proposed Radar investigates and demonstrates the cyclostationary algorithm at the operating frequency of 5.8 GHz, using a Software Defined Radio (SDR) platform for monitoring breathing and heartbeat frequency. A simulation prototype has been implemented in GNU Radio- companion 3.9.5 in Ubuntu 22.04 machine, combined with Python block to verify the detection performance of the proposed system.

The principle of bio-radar for monitoring vital signs is based on phase modulation induced by mechanic movement of the thorax. The human chest wall has a variable position over time, due to respiration and heart rate. The thoracic displacement varies between 4 mm and 12 mm due to respiration, while it varies between 0.2 mm and 0.5 mm due to heartbeat. To accurately estimate RR and HR, various signal processing techniques have been used, including the theory of cyclostationarity. This theory makes it possible to estimate and detect vital signs without demodulation and at a low Signal-to-noise ratio (SNR) in the presence of interference. We have developed second-order cyclic statistics. The flowchart in Figure 1 describes the different steps carried out in the simulation part for the generation of the signal reflected by the antenna and the associated processing, to extract RR and HR. The enhanced visibility of the HR post-harmonic suppression suggests improved clarity in isolating and detecting cardiac features. The effectiveness of the method is reflected in its ability to highlight the HR despite the presence of strong respiratory harmonics.

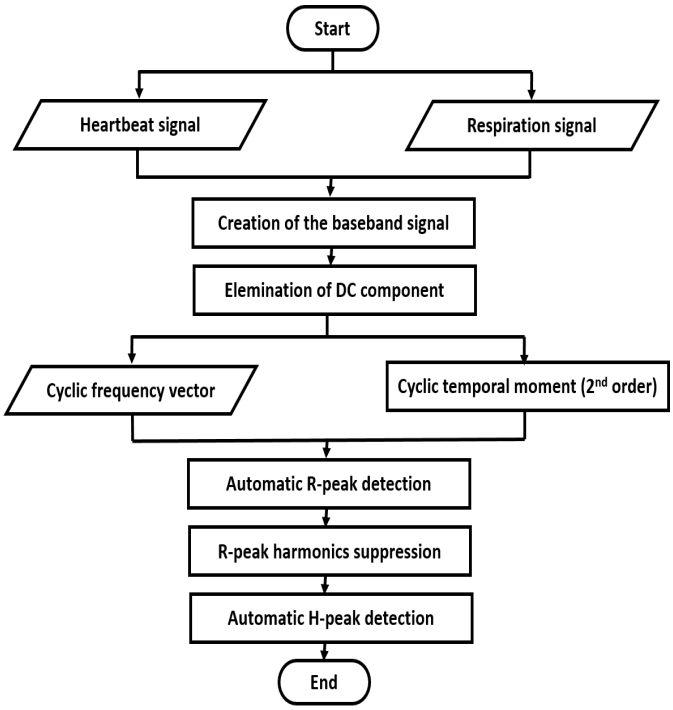

FIGURE 1: General diagram of the simulated algorithm to extract RR and HR

The transmitted signal on the CW channel, operating at frequency f, and serving as the local oscillator, can be expressed as:

$$T(t) = \cos\left(2\pi f t + \varphi(t)\right) \tag{1}$$

For simplicity, the physiological signals representing heartbeats x_h and respiration x_r are approximated as sinusoidal waves. The signal reflected by the target at a distance d_0 is formulated as:

$$R(t) = A_{HR}\cos[2\pi f t - \frac{4\pi d_0}{\lambda} - \frac{4\pi x_{HR}(t)}{\lambda} - \frac{4\pi x_I(t)}{\lambda} + \varphi(t - \frac{2d_0}{c})] + N(t) \tag{2}$$

Where $x_I(t)$ is the random body motion and the propagating electromagnetic wave travels the distance $2d(t)$, and $d(t) = d_0 + x_{HR}(t) + x_I(t)$.

Furthermore, the baseband signal, as depicted in the flowchart, can be simplified into its complex representation, as described in [27]:

$$B_b(t) = AM(t)\sum_{q=-\infty}^{\infty}\sum_{l=-\infty}^{\infty} j^{q+l}J_q(A_r)J_l(A_h) \; exp\left[j2\pi(qf_r + lf_h)t\right] + Z(t) \tag{3}$$

Where:

$$A = A_{HR}exp(j\frac{4\pi d}{\lambda}) \tag{4}$$

$$M(t) = exp\left[j(\frac{4\pi x_I(t)}{\lambda} + \Delta\varphi\,(t))\right] \tag{5}$$

A signal is wide-sense almost-cyclostationary of order m if its statistics of order m, such as moments and cumulants, are almost periodic functions of time [29]. Our focus lies in extracting the cyclostationary second-order temporal cyclic moments of the received baseband signal (3) to detect RR and HR.

To approximate the real measurement environment for this signal, we need to consider the effects of multipath propagation and noise. To incorporate multipath effects into signal models, complex formulations are necessary. These formulations involve accounting for reflections from multiple paths, each characterized by its amplitude, phase, and delay. Moreover, modulation and phase shifts induced by the transmission and environmental conditions must also be considered. The model of the baseband signal including the effect of multipath propagation is as follows:

$$B_b(t) = AM(t) \sum_{q=-\infty}^{\infty} \sum_{l=-\infty}^{\infty} j^{q+l} J_q(A_r) J_l(A_h) \exp\left[j2\pi(qf_r + lf_h)t\right] + Z(t) \tag{6}$$

Where $Z(t)$ represents the additional noise introduced in the signal due to the real environment. Additionally, the presence of multipath propagation leads to a distortion in the signal's propagation. This distortion can be accounted for by modifying the amplitude A in the following way:

$$A = A_{HR} \exp\left(j\frac{4\pi d}{\lambda}\right) \cdot H(t) \tag{7}$$

Here, $H(t)$ denotes the multipath propagation effect, which can be represented as a complex function of time capturing the delay and attenuation characteristics imposed by multipath propagation. Incorporating these adjustments provides a more realistic representation of the signal's behavior in practical measurement environments. The expression for the multipath propagation effect $H(t)$ typically involves a convolution of the signal with a channel impulse response, representing the time-domain response of the channel to an impulse input. In the context of wireless communication, this impulse response captures the effects of reflections, diffraction, and scattering from various objects in the propagation environment.

The second-order temporal cyclic moment, also known as the conjugate cyclic autocorrelation function, is defined as follows in reference [4]:

$$R_{yy}(\alpha, \tau) = \lim_{T\to\infty} \frac{1}{T} \int_{\frac{-T}{2}}^{\frac{T}{2}} B_b(t) B_b^*(t+\tau) e^{-j2\pi\alpha t}\, dt \tag{8}$$

Substituting $B_b(t)$ from the provided signal model considering the multipath effect:

$$R_{yy}(\alpha, \tau) = \lim_{T\to\infty} \frac{1}{T} \int_{\frac{-T}{2}}^{\frac{T}{2}} (AM(t) \sum_{q=-\infty}^{\infty} \sum_{l=-\infty}^{\infty} j^{q+l} J_q(A_r) J_l(A_h) \exp\left[j2\pi(qf_r + lf_h)t\right] + Z(t)) \times (AM(t+\tau)^* \sum_{q'=-\infty}^{\infty} \sum_{l'=-\infty}^{\infty} j^{-q'+l'} J_{q'}(A_r) J_{l'}(A_h) \exp[-j2\pi(q' f_r + l' f_h)(t+\tau)] + Z(t+\tau)^*) e^{-j2\pi\alpha t}\, dt \tag{9}$$

Now, let's simplify this expression. We will need to consider the conjugate terms $B_b^*(t+\tau)$ and also note that $Z(t)$ and $Z(t+\tau)$ represent additional noise, which we assume to be independent of the signal. Therefore, the cross-term involving noise will become negligible or effectively eliminated when averaged over a large interval T.

$$R_{yy}(\alpha, \tau) = \lim_{T\to\infty} \frac{1}{T} \int_{\frac{-T}{2}}^{\frac{T}{2}} (\text{signal term} + \text{noise term}) e^{-j2\pi\alpha t}\, dt \tag{10}$$

After further simplification and dropping the noise term, we'll get:

$$R_{yy}(\alpha, \tau) = A^2 R_M(\tau) \sum_{q=-\infty}^{\infty} \sum_{l=-\infty}^{\infty} \sum_{q'=-\infty}^{\infty} \sum_{l'=-\infty}^{\infty} J_q(A_r) J_l(A_h) J_{q'}(A_r) J_{l'}(A_h) exp\left[-j2\pi(q' f_r + l' f_h)\tau\right] \delta(\alpha - ((q'-q)f_r + (l'-l)f_h)) + R_Z(\tau) \tag{11}$$

In the derived expression for the second-order temporal cyclic moment $R_{yy}(\alpha, \tau)$, we have incorporated the multipath effects and modulation within the signal. However, the exact form of this expression would depend on the specific properties of $M(t)$, $H(t)$, $Z(t)$, and other parameters involved. Provided that $R_M(\tau) \neq 0$, the conjugate cyclic autocorrelation function of $B_b(t)$ is defined for the set of cyclic frequencies $A_\alpha = \{\pm((q'-q)f_r + (l'-l)f_h), 0\}$. Let's break down the expression and interpret the various components:

$A^2 R_M(\tau)$: A represents the complex amplitude of the signal, accounting for both the original signal amplitude and the multipath propagation effect. And $R_M(\tau)$ represents the cyclic autocorrelation function of the modulation term $M(t)$ which includes the effects of both random body motion and phase shifts induced by transmission and environmental conditions.

$J_q(A_r) J_l(A_h) J_{q'}(A_r) J_{l'}(A_h)$: These terms represent the Bessel functions applied to the amplitudes of heart rate (A_h) and respiration (A_r). Bessel functions account for the modulation imposed by heart rate and respiration on the signal.

$exp\left[-j2\pi(q' f_r + l' f_h)\tau\right]$: This exponential term represents the phase modulation imposed by heart rate and respiration frequencies on the signal.It accounts for the cyclic nature of the signal due to heart rate and respiration.

$\delta(\alpha-((q'-q)f_r+(l'-l)f_h))$: This term is the Dirac delta function, enforcing the cyclostationary property of the signal. It ensures that the cyclic frequencies α are constrained by combinations of heart rate and respiration frequencies.

$R_Z(\tau)$: represents the autocorrelation function of the noise term $Z(t)$. It describes the correlation of noise over time delays τ.

III. RAYLEIGH CHANNEL MODEL

To model multipath effects in vital signs detection at a frequency of 5.8 GHz and short distances, one can utilize the electromagnetic wave propagation model in complex environments. At this frequency and distance, waves undergo several propagation phenomena such as reflection, diffraction, refraction, and scattering [30] caused by a transmitted signal interacting with objects in the environment around the transmitter or receiver Figure 2.

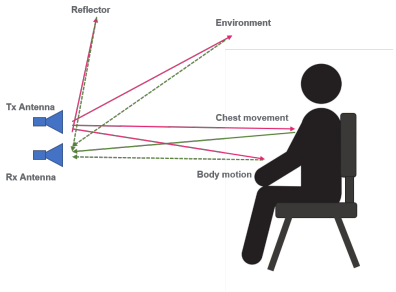

(a)

FIGURE 2: Multipath propagation environments

Different multipath components arrive at the receiver with different time delays and phase shifts. A commonly used model to describe these phenomena is the Rayleigh fading channel model [31]. This model assumes that the received signal is a sum of multiple copies of the transmitted signal, each experiencing different attenuation and delays due to multiple paths. In this model, the amplitudes and phases of the signal's different components are modeled as random variables distributed according to a Rayleigh distribution for amplitude and uniformly distributed for phase.

To apply the Rayleigh fading channel model to the baseband signal for vital signs detection at a frequency of 5.8 GHz and short distances, the received signal $y(t)$ can be expressed as a sum of multiple copies of the transmitted baseband signal $B_b(t)$, each undergoing different attenuation and delays [32]:

$$y(t) = \sum_{i=1}^{N} h_i(t) \cdot B_b(t - \tau_i) + n(t) \tag{12}$$

where: $h_i(t)$ represents the channel impulse response corresponding to the ith path, τ_i is the delay associated with the ith path, N is the total number of paths and $n(t)$ represents additive white Gaussian noise (AWGN).

In the Rayleigh fading channel model, the channel impulse response $h_i(t)$ is typically modeled as a complex Gaussian random process with zero mean and an exponential autocorrelation function, characterized by the Rayleigh fading parameter. The expression for $h_i(t)$ in this case can be represented as [33]:

$$h_i(t) = A_i \cdot \exp(j\phi_i) \cdot g(t) \tag{13}$$

where: A_i is the amplitude of the ith path, following a Rayleigh distribution, ϕ_i is the phase of the ith path, uniformly distributed and $g(t)$ represents the shape of the channel impulse response. This model captures the random nature of multipath propagation, where each path contributes with its amplitude and phase, resulting in fluctuations in the received signal's strength and phase over time.

IV. RADAR FOR RR AND HR DETECTION: SIMULATION

In GNU Radio, programming entails visually creating block diagrams, which encapsulate data processing algorithms. The generation of the baseband signal and the execution of the cyclostationary algorithm were achieved through Python blocks. Figure 3 depicts the GNU block diagrams.

Figure 4 shows the simulation results in the cyclic frequency domain. It represents the second cyclic temporal moment of the baseband signal, both before and after the elimination of the RR harmonics. The interval corresponds to an adult's normal respiratory rate, ranging from 0.16 Hz to 0.44 Hz. Thus, the cyclic frequency corresponds to the maximum amplitude frequency in this interval is attributed to the RR. After removing the breath harmonics, we focus on the interval between 0.83 Hz and 1.6 Hz corresponding to the heart rate. The HR is attributed to the frequency corresponding to the maximum amplitude in this interval [4].

The figures display cyclic statistics containing both heart and respiration frequencies ($f_h = 1.3$ Hz and $f_r = 0.25$ Hz) along with combinations of frequencies describing each order. Initial Dominance of RR Harmonics: The presence of strong harmonics related to the respiratory rate initially overshadowed the fundamental frequency of HR. Before suppressing RR harmonics, the first harmonic of RR ($2f_r = 0.5$ Hz) appears more prominent than the fundamental frequency of HR. After suppressing the RR harmonics, the HR becomes more apparent and noticeable compared to the initial representation. Enhanced HR Visibility with the deleting of the RR harmonics has led to improved visibility and prominence of the heart rate in the cyclic features.

In the figures of cyclic features, all the cyclic statistics contain the heart and respiration frequencies, $f_h = 1.3Hz$ and $f_r = 0.25Hz$, and all the frequencies combination that describes each order. Before the suppression of the RR harmonics, the first harmonic of RR $2 * f_r = 0.5Hz$ is more important than the fundamental of HR. After the suppression of the RR harmonics, we can see that the HR

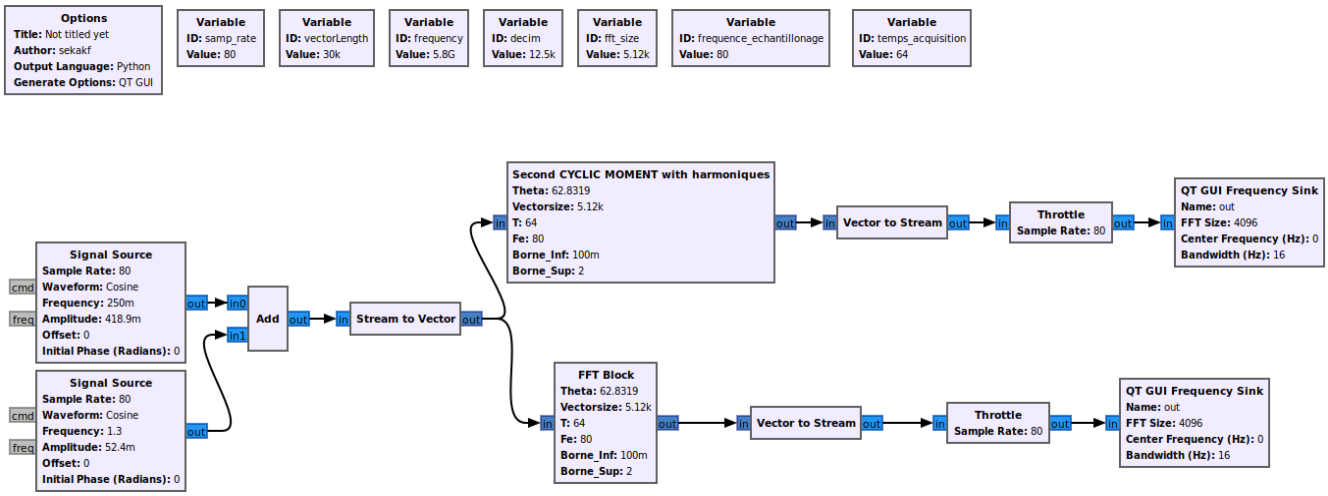

FIGURE 3: Radio Flow graph used for the simulation

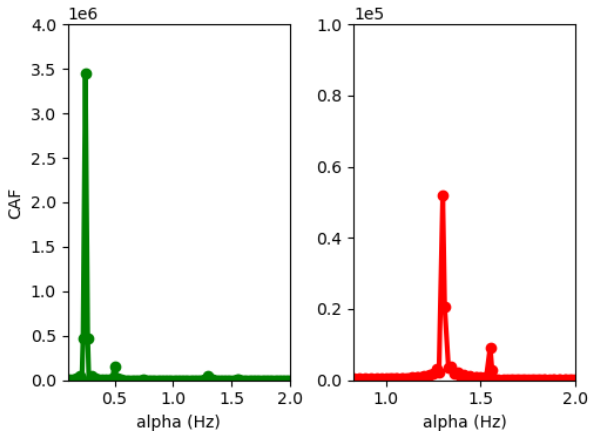

(a)

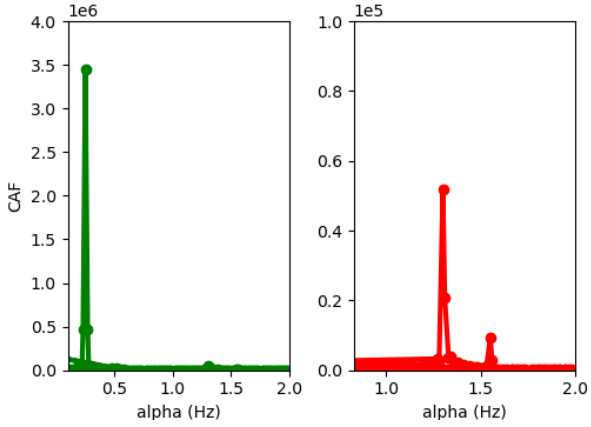

(b)

FIGURE 4: 2^{nd} order cyclic moment of $B_b(t)$: (**a**) before and (**b**) after the suppression of the R-harmonics

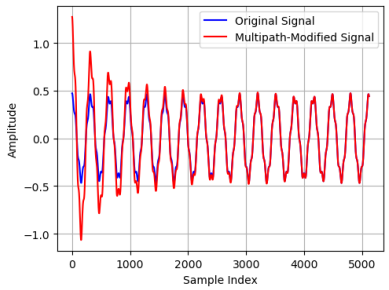

(a)

FIGURE 5: Comparison of Original and Multipath- Radar Signals

is more obvious than before. Multipath propagation occurs when radar signals encounter obstacles or reflect off surfaces, leading to multiple signal paths reaching the receiver with different delays, amplitudes, and phases. The received signal over a multipath channel can be modeled as the convolution between the channel impulse response and the transmitted signal.

This section will provide a comparison between the Fast Fourier Transform (FFT), commonly used for non-contact monitoring of vital signs, and the cyclostationary algorithm. The FFT is a widely used algorithm for analyzing the frequency content of signals. It transforms a time-domain signal into its frequency components. In our study, we employed a sampling frequency of 80 Hz for signal acquisition. For the FFT analysis, we utilized the predefined FFT function in Python, which uses a rectangular window by default.

The FFT assumes signal stationarity during the analysis window, which might not be suitable for signals with time-varying characteristics, such as vital signs. In contrast, cyclostationary analysis is designed to capture and exploit the cyclostationary nature of signals, making it more suitable

This article has been accepted for publication in IEEE Open Journal of Instrumentation and Measurement. This is the author's version which has not been fully edited and content may change prior to final publication. Citation information: DOI 10.1109/OJIM.2024.3502888

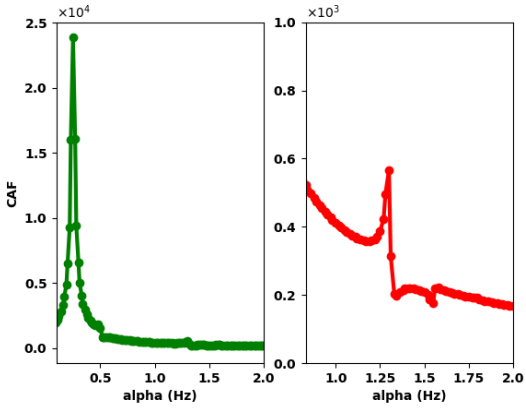

(a)

FIGURE 6: 2^{nd} order cyclic moment of $B_b(t)$ with multipath effect

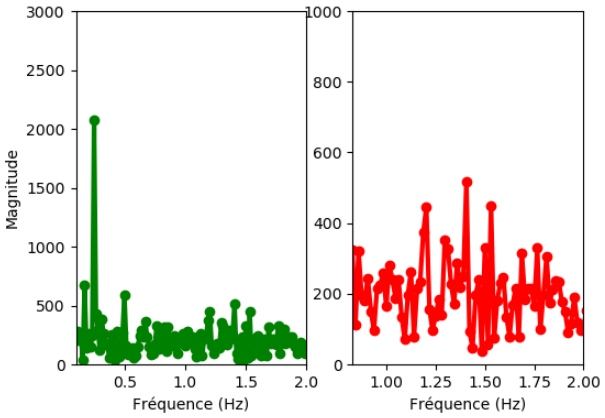

(a)

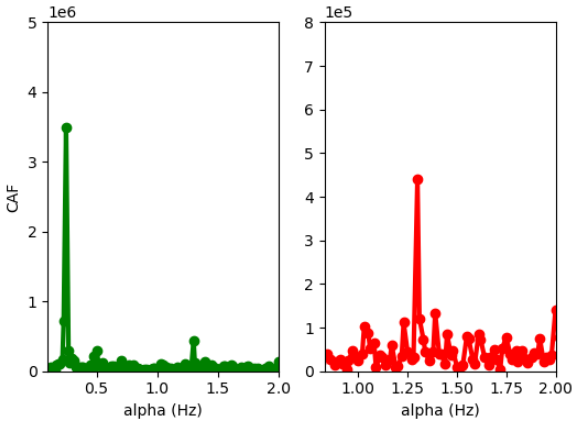

(b)

FIGURE 7: (**a**) FFT analysis and (**b**) CAF function

for non-stationary varying vital signs. The results of the detection of respiratory rate (RR) and heart rate (HR) using both algorithms (second cyclic moment for cyclostationary analysis and FFT) are depicted in Figure 7. Cyclostationary algorithms can detect weak periodic signals even in low signal-to-noise ratio (SNR) environments. They can detect vital signs even in the presence of random body movements that often interfere with FFT-based detection. While FFT remains a valuable tool for its simplicity and efficiency, cyclostationary algorithms offer significant advantages in challenging real-world conditions, especially for extracting the heart rate.

To further evaluate the influence of noise on the detection of vital signs, we conducted simulations to calculate the probability of detection concerning the signal-to-noise ratio (SNR). In this simulation, we examined whether the estimated values (f_h' and f_r') for HR and RR align with the originally set values for the transmitted signals (f_h and f_r). This comparison illustrated in Figure 8 serves as a validation step to assess the accuracy of the algorithm in estimating RR and HR varying levels of noise.

The probability of detection for f_r is consistently 1 for all levels of SNR and for both algorithms, it indicates that the algorithm is effectively detecting the respiratory signal in the presence of noise. This outcome is because the respiratory signal is the strongest component of the baseband signal. The heart rate detection is around 0.85 for each distance value. On the other hand, the probability of detection of the heart rate using the cyclostationarity algorithm increases with the SNR. The FFT may be sensitive to noise and might not perform well in the presence of irregularities. While the cyclostationarity analysis is often more robust against noise and interference conditions, which are common obstacles in non-contact vital signs monitoring. This is a positive outcome to evaluate the algorithm's performance under different conditions.

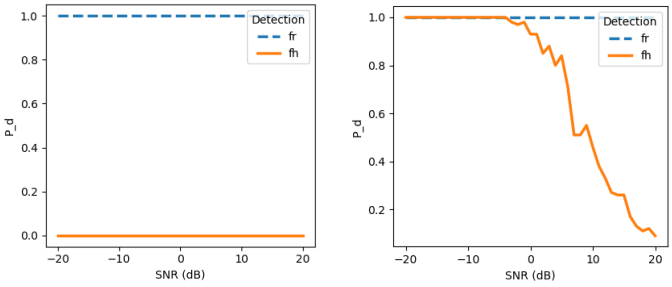

(a) (b)

FIGURE 8: Probability of detection of RR and HR using: (**a**) FFT analysis and (**b**) second-order cyclostationarity algorithm

V. RADAR FOR RR AND HR DETECTION: EXPERIMENTAL SETUP

In this section, we detail the experimental configuration proposed for validating the 5.8 GHz radar system. The system is constructed using Universal Software Radio Peripheral (USRP) 2901 devices. Illustrated in Figure 10, the board features a 4-channel transmitter/receiver and primarily integrates a wideband RF transceiver and an FPGA. The examined board covers a frequency range from 70 MHz to 6 GHz, has a gain range of 66 dB, and boasts a maximum instantaneous real-time bandwidth of approximately 56 MHz. The transmitter outputs a maximum power of 20 dBm, while the receiver accommodates a maximum input power of -15 dBm [**?**]. In addition to the non-contact radar system, we employed a contact-based measurement device, a pulse oximeter (9), to obtain reference values for heart rate and respiratory rate. The pulse oximeter was attached to the subject's finger throughout the experiments. The simultaneous use of the pulse oximeter allowed for direct comparison between our non-contact 5.8 GHz radar system and the reference values, ensuring the reliability and accuracy of our proposed method.

FIGURE 9: Pulse oximeter used for RR and RH reference

The measurement bench setup comprises a USRP card featuring two RF channels. In channel zero, the transmitter port (Tx1 Rx1) is linked to the transmitter antenna, and the receiver port (RX2) is connected to an attenuator, further linked to the receiver antenna. A 10 dB RF attenuator is incorporated to shield the receiver from excessively high input power and high signals. The USRP is connected to a laptop via a USB cable. The laptop has an i7-core processor and 8G RAM, and runs the program written in GNU Radio version 3.9.5 in Ubuntu 22.04 and Python blocks to extract RR and HR. The bench architecture operating at 5.8 GHz has two proposed setups. The first proposal employs two horn antennas shown in Figure 11, while the second uses two patch antennas developed in our laboratory demonstrated in Figure 12. The radar prototype used in both cases is presented in the two figures 11 and 12, along with the radiation pattern of each antenna used.

In our study, the radiation patterns of both the horn antenna and the patch antenna in our system were measured in the anechoic chamber with dimensions of 7×6.5×2.4m, focusing on far-field measurements at the frequency of 5.8 GHz. The anechoic chamber replicates free-space propagation conditions by eliminating all reverberations of the

(a)

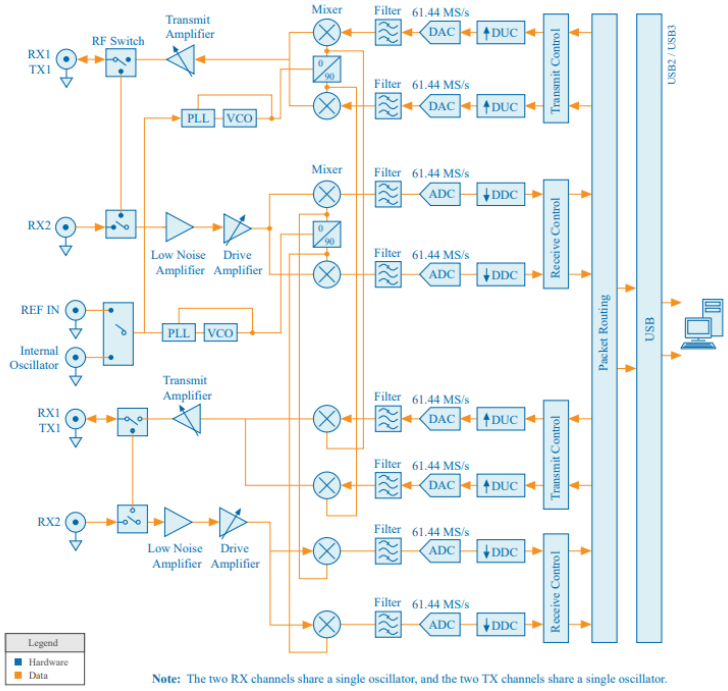

(b)

FIGURE 10: USRP-2901 Block Diagram

incident waves, achieved through absorbing materials that cover the chamber's walls, ceiling, and floor. The radiation pattern was obtained by positioning the patch antenna on a rotating platform and measuring the signal received by the horn antenna. The horn antenna used for measuring the S-parameters of the patch antenna is a wideband antenna, capable of operating across a broad frequency range from 700 MHz to 18 GHz. The same measurement protocol was employed to obtain the radiation pattern of the horn antenna at 5.8 GHz.

- Test bench 1: USRP card + two patch antennas at 5.8 GHz
- Test bench 2: USRP card + two horn antennas at 5.8 GHz

The measurements are performed using the microwave signal generated on the GNU Radio software and sent through the USRP card to the transmitting antenna. In transmission, this continuous signal has targeted a

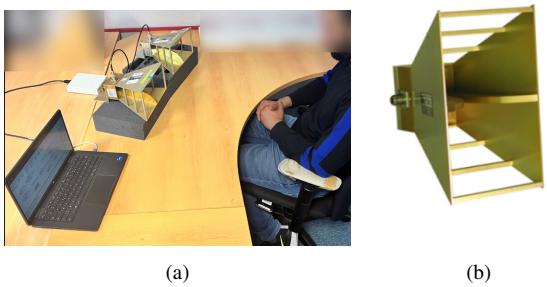

(a) (b) (c)

FIGURE 11: (**a**) Test bench 2 with the horn antennas, (**b**) the horn antenna and (**c**) its radiation pattern at the 5.8 GHz

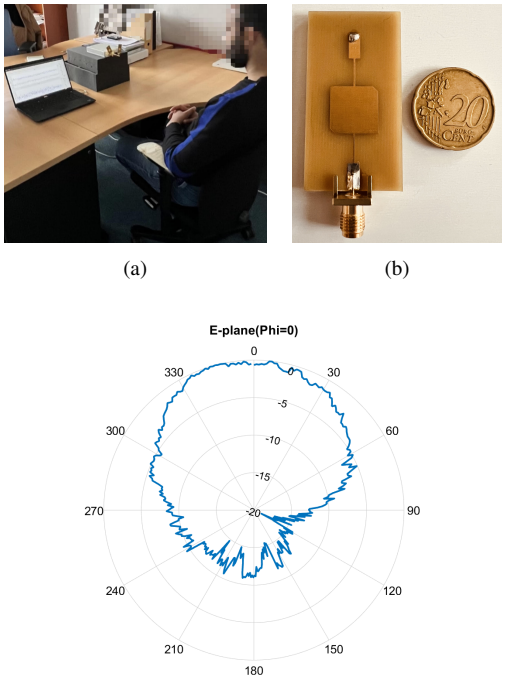

(a) (b) (c)

FIGURE 12: (**a**) Test bench 1 with the patch antennas, (**b**) the patch antenna and (**c**) its radiation pattern at the 5.8 GHz

mechanical and periodic movement of the chest's subject under test. On reception, the wave has been picked up by the receiving antenna, directed to the USRP receiver, and visualized on the GNU Radio platform. To evaluate the performance of the developed systems, a series of tests were carried out on five volunteer subjects wearing their clothes for both systems. The received signal has been converted to low frequencies by Python blocks to apply the second-order algorithm of cyclostationarity to extract the heart rate and respiratory rate parameters. The GNU radio graph used for this experiment is shown in Figure 13.

In a laboratory environment, continuous wave (CW) radar measurements are conducted using the USRP platform. Subjects wear the oximeter and sit in front of the radar system with a distance of 0.8 to 1 meter between their chest and the antenna board. The radar signals collected in the laboratory environment are affected by noise, including electronic noise from the radar system and environmental noise. Additionally, multipath effects due to reflections, diffraction, and scattering from surrounding objects influence the characteristics of the received signals. Then, signal processing techniques based on a second-order cyclic moment of the measured signals are employed to extract relevant information from the measured radar signals, which provides insights into the cyclostationary nature of the received signals and the estimations of the RR and HR. The five healthy participants (2 females and 3 males) between the ages of 19 and 37 wearing the oximeter to have the reference values for RR and HR. In the upcoming sections, we will show the figures for two subjects: the first subject is male, and the second subject is female.

The initial phase of the experiment utilized the first test bench, as illustrated in Figure 12, for all subjects. The reflected signals, influenced by the chest displacement, were captured by the board and are depicted in Figure 14 and Figure 16 for the first and second subjects, respectively. These signals are complex, with real and imaginary components. Employing Python, the signals were down-converted to baseband and had their DC bias removed. Subsequently, the second-order cyclostationary algorithm was applied, presented as a function of the cyclic frequencies defined for the second-order. The results are illustrated in Figure 15 and Figure 17 for the first and second subjects, respectively.

In the second phase of the measurement, the patch antennas in test bench 2 (Figure 11) were substituted with horn antennas for both subjects. Figures 18 and 20 showcase the reflected signals received by the board, modulated by chest displacement. Additionally, Figures 19 and 21 illustrate their second-order cyclic moments for the first and second subjects, respectively.

The time-domain signal exhibits a noticeable periodic pattern in all four mentioned cases. It is essential to recognize that this received signal encapsulates information

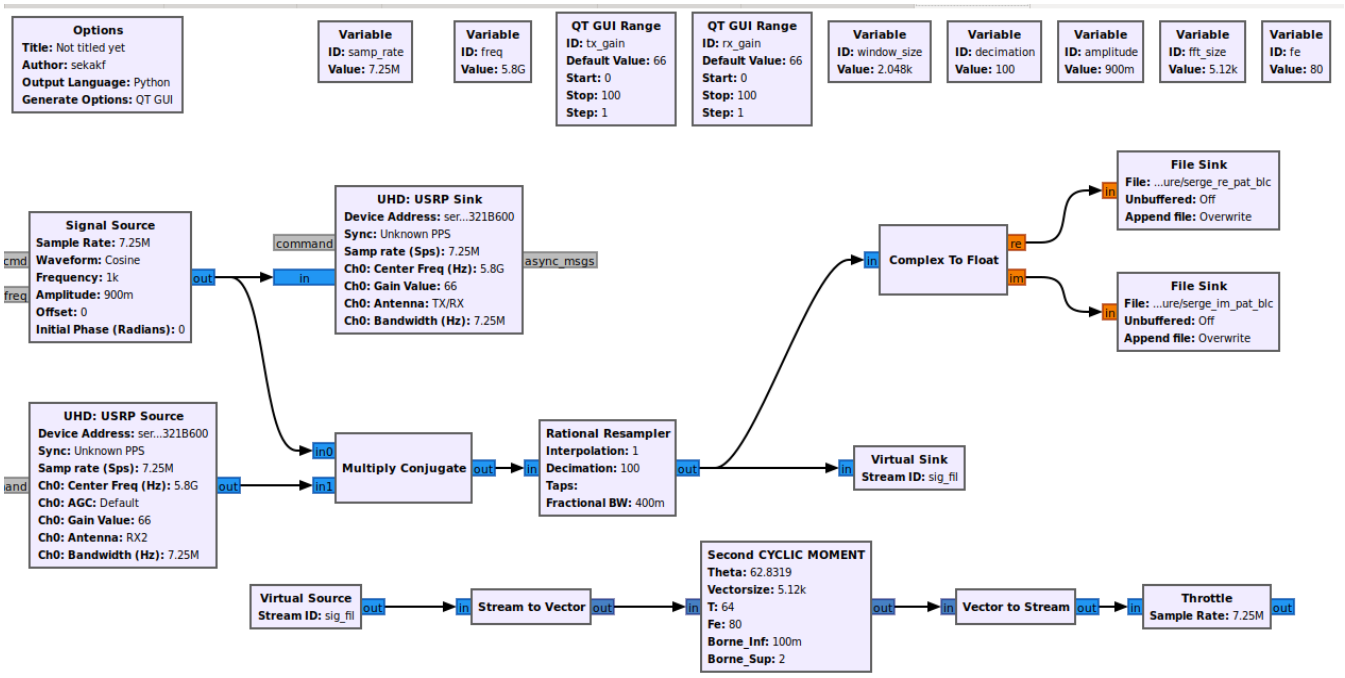

FIGURE 13: GNU radio flowgraph for the CW Radar

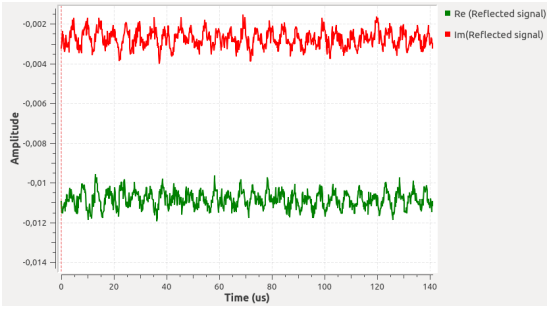

FIGURE 14: Received signal in the time domain: Test bench 1 for the subject 1

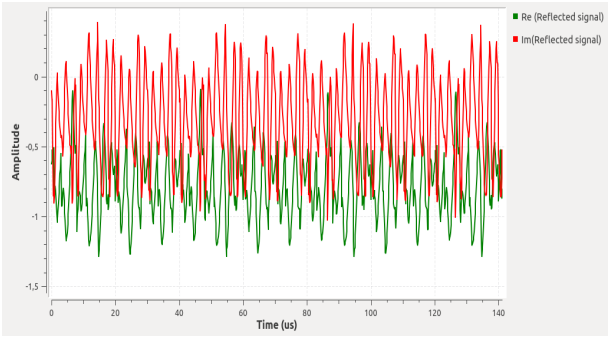

FIGURE 16: Received signal in the time domain: Test bench 1 for the subject 2

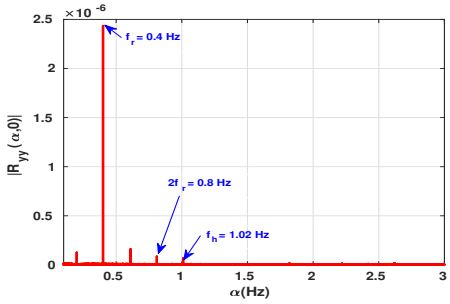

FIGURE 15: Second cyclic temporal moment of the received signal: Test bench 1 for the subject 1

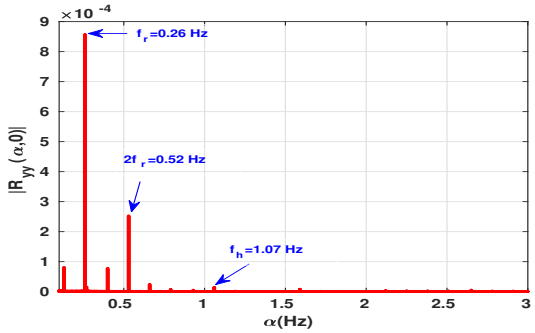

FIGURE 17: Second cyclic temporal moment of the received signal: Test bench 1 for the subject 2

regarding both the displacement caused by breathing and the displacement induced by the heartbeat. Therefore, it

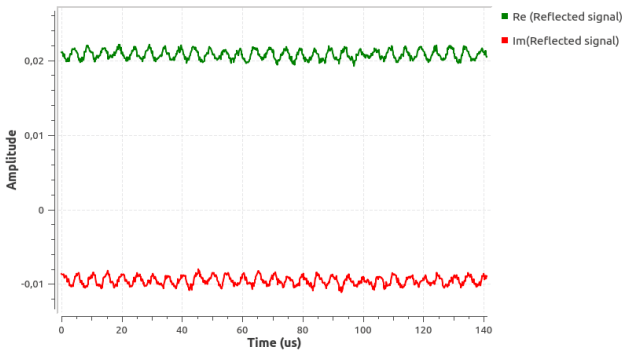

FIGURE 18: Received signal in the time domain: Test bench 2 for the subject 1

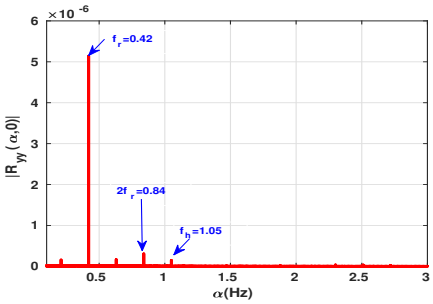

FIGURE 19: Second cyclic temporal moment of the received signal: Test bench 2 for the subject 1

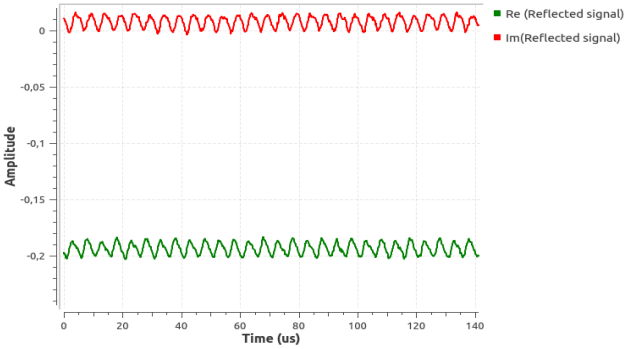

FIGURE 20: Received signal in the time domain: Test bench 2 for the subject 2

represents the cumulative effect of the overall displacement over the chest area of the subject under examination. It is normal for the magnitude of the received signal to vary among the cases. The horn antenna, although more directive, and the patch antenna, being smaller, offer distinct advantages suitable for integration into diverse prototypes in different environments. In the case of the first subject, the peak of the respiratory rate is approximately 0.4 Hz for both test benches.

In the case of the first subject, the peak of the respiratory rate is observed at 0.4 Hz for the first test bench and 0.42

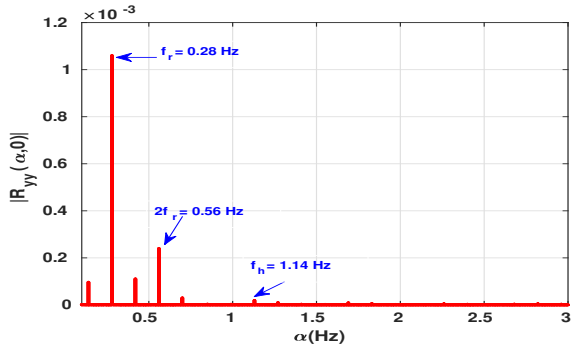

FIGURE 21: Second cyclic temporal moment of the received signal: Test bench 2 for the subject 2

Hz for the second test bench. For the second subject, the respiratory rate is approximately 0.26 Hz for the first test bench and 0.28 Hz for the second test bench. Table 1 and Table 1 resume the results of the RR and HR for the five participants with both system non-contact and with contact to compare the values from the test bench 1 and test bench 2, respectively. The mean relative error is calculated for RR and HR.

TABLE 1: Comparison between the detection of RR and HR resulting from the cyclostationarity algorithm and the reference system for the test bench 1

	Cyclostationarity		Pulse oximeter		Relative Error (%)	
Participant	RR (Hz)	HR (Hz)	RR (Hz)	HR (Hz)	RR (Hz)	HR (Hz)
Male 1	0.4	1.02	0.4	1.09	2.4	5.6
Female 1	0.26	1.07	0.3	1.1		
Male 2	0.35	1.1	0.34	1.15		
Male 3	0.31	1.2	0.35	1.25		
Female 2	0.33	1.12	0.3	1.2		

TABLE 2: Comparison between the detection of RR and HR resulting from the cyclostationarity algorithm and the reference system for the test bench 2

	Cyclostationarity		Pulse oximeter		Relative Error (%)	
Participant	RR (Hz)	HR (Hz)	RR (Hz)	HR (Hz)	RR (Hz)	HR (Hz)
Male 1	0.42	1.05	0.44	1	1.8	4.6
Female 1	0.28	1.14	0.3	1.2		
Male 2	0.4	1.35	0.37	1.4		
Male 3	0.3	1.08	0.32	1.1		
Female 2	0.3	1.3	0.3	1.35		

The estimated values of RR showed consistency between the two systems benches, demonstrating the reliability of the non-contact monitoring method. However, It was observed that the respiratory rate had a more pronounced influence on the signal than the heart rate (HR). This dominance of RR presents a significant challenge in the detection of HR, particularly in instances where the first harmonic of the respiratory rate surpasses the peak of the heart rate. Despite these challenges, all HR values obtained by the cyclostationarity and oximeter algorithms were close and within normal ranges for each case, indicating the potential validity of the heart rate measurements. Analysis of the cyclic frequencies revealed distinct RR peaks for both test benches. In test bench 1, RR peaks were identified at 1.02 Hz and 1.07 Hz for the first and second subjects, respectively. For test bench 2, the peaks were found at 1.05 Hz and 1.14 Hz for the first and second subjects, respectively. These results highlight the system's ability to detect subtle differences in breathing rates between subjects.

To assess the accuracy of the non-contact system, the relative error between the HR and RR measurements obtained from the cyclostationarity-based analysis and the pulse oximeter reference was calculated. The observed differences in estimated RR and HR values between the two measurement systems can be attributed to various factors, including the age, weight, and sex of the subjects, as well as individual physiological variations. It's important to note the physiological relationship between heart and respiratory rates. Generally, an increase in heart rate corresponds to an increase in respiratory rate. As the heart beats faster, it consumes more energy and requires more oxygen, leading to an increased breathing rate. This relationship was particularly evident in the case of the second subject, who exhibited higher rates for both HR and RR.

Furthermore, technical factors also contributed to the differences in measurements between the two systems. The directivity of the antennas varied between the systems, potentially affecting signal reception and processing. Additionally, the subjects under test were different for each system, introducing another variable in the comparison. Regardless of these challenges and variables, the study successfully demonstrated that both respiratory rate and heart rate could be accurately estimated using Software-Defined Radio (SDR) measurements in a real-world environment. This was achieved using two different prototypes operating at a frequency of 5.8 GHz, showcasing the robustness and versatility of the non-contact monitoring approach combining the USRP card and the second cyclic moments algorithms. These studies may represent the beginning of expanding the range of individuals tested, and it has enabled a comparison of the performance of the system used to study in the future multiple people in front of the radar, allowing for the differentiation of each individual's vital signs.

VI. CONCLUSION

This paper investigates and validates the ability to monitor heart and breathing rates by detecting chest movements. The experimental setup utilized a USRP card developed in GNU Radio, and the second cyclic moment algorithm applied to the reflected signal from the individual was described and analyzed. The results obtained using the second-order cyclostationary approach, in conjunction with the USRP device, are promising for both types of antenna horn and patch across all subjects. The results highlight the performance comparison to have multiple people studies in the future. The method demonstrated robustness in the presence of noise, interference, and multipath effects, as tests were conducted in an uncontrolled environment (laboratory). RR and HR were correctly estimated using the USRP2901 at a frequency of 5.8 GHz, along with GNU Radio and Python blocks. The cyclostationary analysis proved effective in handling non-stationary signals and noisy conditions, making it suitable for complex monitoring environments. Overall, non-contact monitoring offers several advantages, including improved comfort, reduced health risks, and continuous, reliable health data, which are essential for enhancing health outcomes and quality of life, particularly for the elderly. These findings have significant implications for non-contact vital sign monitoring, demonstrating the potential to develop reliable, non-invasive methods for measuring key physiological parameters. Future research could focus on refining algorithms to better differentiate between respiratory and heart rate signals, especially in cases where their frequencies overlap. Additionally, adaptive systems that account for individual physiological differences could further enhance the accuracy and reliability of these non-contact monitoring techniques for better classification.

ACKNOWLEDGMENT

The present research work has been supported by Segula Technologies. Segula is an Engineering and Design Services company serve Automotive, Rail and Medical sectors, with expertise in Product Development, Mechanisms and Bio-Medical Engineering Solutions.

REFERENCES

[1] J. C. Lin, "Noninvasive microwave measurement of respiration," *Proceedings of the IEEE*, vol. 63, no. 10, pp. 1530–1530, 1975.

[2] H. Jeong, D. Kim, G. Kim, and S. Kim, "Vitrad: A low-cost continuous wave doppler radar system with 3d-printed horn antennas for human vital sign detection," *HardwareX*, vol. 12, 2022.

[3] S. M. Islam, N. Motoyama, S. Pacheco, and V. M. Lubecke, "Non-contact vital signs monitoring for multiple subjects using a millimeter wave fmcw automotive radar," in *2020 IEEE/MTT-S International Microwave Symposium (IMS)*. IEEE, 2020, pp. 783–786.

[4] F. Sekak, "Microwave radar techniques and dedicated signal processing for vital signs measurement," Ph.D. dissertation, Université de Lille, 2021.

[5] M. Brulc, T. Deleruyelle, A. Loussert, P. Laurent, R. Grisot, and J.-P. Caruana, "Cardiac signature detection and study using contactless technology: Millimeter wave fmcw radar," *IEEE Open Journal of Instrumentation and Measurement*, 2023.

[6] W. Hu, Z. Zhao, Y. Wang, H. Zhang, and F. Lin, "Noncontact accurate measurement of cardiopulmonary activity using a compact quadrature doppler radar sensor," *IEEE Transactions on Biomedical Engineering*, vol. 61, no. 3, pp. 725–735, 2013.

[7] D. Obeid, S. Sadek, G. Zaharia, and G. E. Zein, "Noncontact heartbeat detection at 2.4, 5.8, and 60 ghz: A comparative study," *Microwave and Optical Technology Letters*, vol. 51, no. 3, pp. 666–669, 2009.

[8] G. Vinci, T. Lenhard, C. Will, and A. Koelpin, "Microwave interferometer radar-based vital sign detection for driver monitoring syst," in *2015 IEEE MTT-S International Conference on Microwaves for Intelligent Mobility (ICMIM)*. IEEE, 2015, pp. 1–4.

[9] A. Koelpin, F. Lurz, S. Linz, S. Mann, C. Will, and S. Lindner, "Six-port based interferometry for precise radar and sensing applications," *Sensors*, vol. 16, no. 10, p. 1556, 2016.

[10] F. Khan and S. H. Cho, "A detailed algorithm for vital sign monitoring of a stationary/non-stationary human through IR-UWB radar," *Sensors*, vol. 17, no. 2, p. 290, 2017.

[11] N. V. Rivera, S. Venkatesh, C. Anderson, and R. M. Buehrer, "Multi-target estimation of heart and respiration rates using ultra wideband sensors," in *2006 14th European Signal Processing Conference*. IEEE, 2006, pp. 1–6.

[12] I. Choi, M. Kim, J. Choia, J. Park, S. Parkb, and K. Kimc, "Robust cardiac rate estimation of an individual," *IEEE Sensors Journal*, 2021.

[13] N. Zhu, B. Liu, R. Qi, Z. Chen, S. Xu, and G. Niu, "Vital signs monitoring using an ir-uwb radar based on edge computing," 2021.

[14] S. Costanzo, F. Spadafora, A. Borgia, H. Moreno, A. Costanzo, and G. Di Massa, "Research article high resolution software defined radar system for target detection," 2013.

[15] P. Sharma, Z. Zhang, T. B. Conroy, X. Hui, and E. C. Kan, "Attention detection by heartbeat and respiratory features from radio-frequency sensor," *Sensors*, vol. 22, no. 20, p. 8047, 2022.

[16] S. Costanzo, F. Spadafora, G. Di Massa, A. Borgia, A. Costanzo, G. Aloi, P. Pace, V. Loscri, and H. O. Moreno, "Potentialities of usrp-based software defined radar systems," *Progress In Electromagnetics Research B*, vol. 53, 2013.

[17] D. Y. C. Lie, Y. Liu, Y. Tchatchoua, C. Sweeney, P. E. Lie, and T. Q. Nguyen, "Latest development on non-contact vital signs (ncvs) sensor systems using software defined radio (sdr)," in *2021 IEEE 14th International Conference on ASIC (ASICON)*, 2021, pp. 1–4.

[18] W. Li, B. Tan, and R. J. Piechocki, "Non-contact breathing detection using passive radar," in *2016 IEEE International Conference on Communications (ICC)*. IEEE, 2016, pp. 1–6.

[19] A. Raffo, S. Costanzo, and G. Di Massa, "Software defined doppler radar as a contactless multipurpose microwave sensor for vibrations monitoring," *Sensors*, vol. 17, no. 1, p. 115, 2017.

[20] X. Hui and E. C. Kan, "Monitoring vital signs over multiplexed radio by near-field coherent sensing," *Nature Electronics*, vol. 1, no. 1, pp. 74–78, 2018.

[21] S. Costanzo, "Software-defined doppler radar sensor for human breathing detection," *Sensors*, vol. 19, no. 14, p. 3085, 2019.

[22] M. B. Khan, M. Rehman, A. Mustafa, R. A. Shah, and X. Yang, "Intelligent non-contact sensing for connected health using software defined radio technology," *Electronics*, vol. 10, no. 13, p. 1558, 2021.

[23] A. M. A. Ashleibta, "Design of software defined radio based testbed for smart healthcare," Ph.D. dissertation, University of Glasgow, 2022.

[24] I. Lenz, J. Holtom, A. Herschfelt, Y. Rong, and D. Bliss, "Respiratory and heart rate detection using continuous-wave radar testbed implemented in gnu radio," in *Proceedings of the GNU Radio Conference*, vol. 7, no. 1, 2022.

[25] O. Toker and R. Adla, "A sub-6 ghz vital signs sensor using software defined radios," *Engineering Proceedings*, vol. 2, no. 1, p. 38, 2020.

[26] Y. Liu, C. Sweeney, J. Hawkins, S. Rojas, J. Mayeda, Y. Tchatchoua, T. Nguyen, and D. Lie, "Design of a robust noncontact vital signs (ncvs) monitoring system using software defined radio (sdr)," in *2021 IEEE Texas Symposium on Wireless and Microwave Circuits and Systems (WMCS)*. IEEE, 2021, pp. 1–4.

[27] F. Sekak, K. Zerhouni, F. Elbahhar, M. Haddad, C. Loyez, and K. Haddadi, "Cyclostationary-based vital signs detection using microwave radar at 2.5 ghz," *Sensors*, vol. 20, no. 12, p. 3396, 2020.

[28] F. Sekak, F. Elbahhar, and M. Haddad, "Vital signs detection based on the third order cyclic temporal moment and cumulant," *IEEE Access*, 2022.

[29] W. A. Gardner, A. Napolitano, and L. Paura, "Cyclostationarity: Half a century of research," *Signal Processing*, vol. 86, no. 4, pp. 639–697, 2006.

[30] M. Mercuri, Y. Lu, S. Polito, F. Wieringa, Y.-H. Liu, A.-J. van der Veen, C. Van Hoof, and T. Torfs, "Enabling robust radar-based localization and vital signs monitoring in multipath propagation environments," *IEEE Transactions on Biomedical Engineering*, vol. 68, no. 11, pp. 3228–3240, 2021.

[31] N. T. Phuoc Van, L. Tang, S. C. Mukhopadhyay, D. M. Nguyen, and F. Hasan, "Probabilities of false alarm for vital sign detection on the basis of a doppler radar system," *Sensors*, vol. 18, no. 3, p. 694, 2018.

[32] T. S. Rappaport, *Wireless communications: principles and practice*. Cambridge University Press, 2024.

[33] A. A. Saleh and R. Valenzuela, "A statistical model for indoor multipath propagation," *IEEE Journal on selected areas in communications*, vol. 5, no. 2, pp. 128–137, 1987.

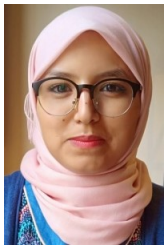

Fatima SEKAK received in 2017 the MSc in Intelligent Communicating Systems from the National School of Applied Sciences of Fes, Morocco. Her master's thesis, conducted at the Institute of Electronics and Systems in Montpellier, France, focused on developing a high-frequency ultrasound-based distance measurement system. She further pursued her academic journey, completing her PhD in Electronics, Microelectronics, Nanoelectronics, and Microwaves at the University of Lille in 2021. During her doctoral studies, Fatima collaborated with the LEOST (Electronic Wave and Signal Laboratory for Transport) at the University of Gustave Eiffel, IEMN (Institute of Electronics, Microelectronics and Nanotechnology), and Segula Engineering France for the DESIS project. Her research centered on utilizing millimeter radar for real-time measurement of heart and respiratory activity signals, particularly in the context of a driver's behavior. The focus was on Microwave Radar Techniques and specialized signal processing for Vital Signs measurement. Since March 2022, she has been working within the LEOST team at Gustave Eiffel University as a research engineer on the development of a functional system coupled with a data acquisition and processing methodology, enabling real-time analysis and capable of detecting alarming variations in vital signs as a part of "Plan France Relance" with Segula Technologies.

Fouzia ELBAHHAR received the Ph.D. degrees from the University of Valenciennes, France, in 2000 and 2004, respectively. She is currently a Research Director at Gustave Eiffel university. She is also the Research Director. She has participated in many national and European projects dedicated to transport applications. She is involved in signal processing, Radar for vital signs, 5G wireless communication, and cognitive radio. She has authored or co-authored more than 80 research papers, including journal articles, book chapters, and conference proceedings. Her major research interests include indoor positioning, radar, and wireless radio systems. She serves as a Reviewer for several journals and international conferences.

Madjid HADDAD received in 2013 his PhD in Mechanics, during his doctoral studies; Madjid collaborated with the Clement ADER Institute at Toulouse University. His research centred on the mechanical behaviour of manufactured composites materials. In this work, the focus was about the relationship between the induced damages by detouring and the mechanical behaviour of CFRP composites. From 2014 to 2016, he pursued his career as a research engineer with Roberval laboratory at Compiegne University of technology (UTC). The goal was to study the effect of functionalisation of composites martial by adding carbon particles. Since June 2016, he has joined SEG-

ULA engineering as a head of research and development. He constructs, supervises different R&D projects focussing on new technologies such as IA, VR and enhancing existing technologies using novel approaches and developing new solutions.